J|A|C|S
COMMUNICATIONS

Published on Web 11/11/2006

Hybrid Gold/Silica/Nanocrystal-Quantum-Dot Superstructures: Synthesis and Analysis of Semiconductor−Metal Interactions

Nanguo Liu, Bradley S. Prall, and Victor I. Klimov*

Chemistry Division, Los Alamos National Laboratory, Los Alamos, New Mexico 87545

Received August 18, 2006; E-mail: klimov@lanl.gov

Enhancement of light−matter interactions near metal surfaces has been widely utilized in surface-enhanced Raman spectroscopy (SERS).[1] SERS is based on the enhancement of local fields associated with excitation of collective electron oscillations in metals [surface plasmons (SPs)], which can lead to orders-of-magnitude increase of molecular Raman cross-sections. Interactions with SPs can also significantly affect photoluminescence (PL) intensities of light-emitting chromophores. In this case, however, because of the competition between field enhancement and nonradiative damping due to energy transfer to SPs, the proximal metal can either enhance or decrease the PL intensity. Both of these effects have been observed experimentally for, for example, organic dyes and nanocrystal quantum dots (QDs).[2] Potential applications of metal-induced PL quenching/enhancement range from sensing technologies[3] and solid-state lighting[4] to amplification of surface plasmons.[5]

In this Communication, we report on the synthesis and characterization of well-defined hybrid structures that comprise a gold core overcoated with a silica shell, followed by a dense monolayer of colloidal CdSe QDs. The dielectric silica spacer of a controlled thickness provides a simple means for tuning interactions between the QDs and the metal core. We demonstrate switching between PL quenching and enhancement by varying the silica shell thickness. Our synthesis employs a final step of self-assembly of QDs onto the silica shell via simple titration of the QD solution with the prefabricated Au/SiO_2 particles. This approach allows us to perform an accurate quantitative analysis of the effect of a metal on the QD PL intensity.

Hybrid gold/silica/CdSe-QD nanoparticles were synthesized via a multistep procedure, which involved synthesis of gold nanoparticles, gold-particle surface activation, silica-shell deposition, modification of the silica surfaces with $-NH_2$ groups, and final self-assembly of CdSe QDs onto the particle surfaces (Figure 1A). Gold nanoparticle seeds (15 nm in diameter) were prepared according to the standard sodium-citrate reduction method.[6] A seeded growth method was applied to prepare larger particles (up to 45 nm in diameter). To deposit a silica shell, we used a modified version of the procedure reported previously.[7] We found that (3-mercaptopropyl)trimethoxysilane (MPTMS) was better suited for surface activation of gold nanoparticles than (3-aminopropyl)-trimethoxysilane (APTMS) (originally used in ref 7) because of stronger binding of the −SH groups to the gold surfaces. The use of MPTMS also allowed us to reduce the yield of pure silica particles produced by homogeneous nucleation and structures that comprised multiple Au cores.

The silica-coated nanoparticles were treated with APTMS (a silane coupling agent), which reacted with the surface silanol groups to produce silica surfaces functionalized with $-NH_2$ groups. Finally, the surface-modified nanoparticles were dispersed in a tetrahydrofuran (THF) solution of CdSe QDs synthesized via a high-temperature pyrolysis method.[8] Because of strong binding interactions between the CdSe QDs and the $-NH_2$ ligands, the QDs self-assembled onto the surface of the silica shell, resulting in the targeted hybrid gold/silica/CdSe-QD superstructures.

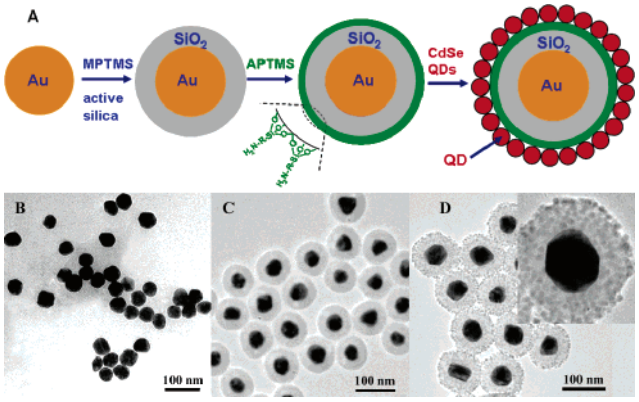

Figure 1. (A) Multistep synthesis of hybrid Au/SiO_2/CdSe-QD nanostructures, (B) TEM images of synthesized gold cores, (C) core/shell gold/silica nanoparticles, and (D) final hybrid Au/SiO_2/CdSe-QD nanostructures (QD diameter is 6.0 nm). Inset is an enlarged image of a single Au/SiO_2/CdSe-QD particle.

Figure 1 shows an example of transmission electron microscopy (TEM) images of gold-core nanoparticles (B), gold/silica core/shell structures (C), and final hybrid gold/silica/QD nanocomposites (D). In this example, the gold-core diameter $D = 45 \pm 4.0$ nm, and the silica-shell thickness $H = 24 \pm 2.4$ nm. While the gold cores have irregular shapes, the gold/silica structures are nearly spherical and highly monodispersed (4% size dispersion). CdSe QDs form uniform dense monolayers on all of the Au/SiO_2 particles. TEM images indicate that our synthesis does not produce such byproducts as plain silica particles or particles comprising multiple Au cores, while such byproducts are difficult to avoid using APTMS as an activator of gold surfaces.

To evaluate the effect of a metal on PL of QDs, we used a dilute solution of CdSe QDs in THF as a reference [original PL quantum yield (QY) is 5%, and the emission wavelength (λ_e) is 630 nm] and measured PL and extinction spectra following titration of this solution with Au/SiO_2−NH_2 particles. In Figure 2A we present the results of these measurements for $D = 45$ nm and $H = 5$ (squares) and 24 nm (circles) shown as raw data (solid symbols) and the data corrected for attenuation of pump radiation ($\lambda_a = 400$ nm) in the sample (open symbols). Both the raw and the corrected data indicate similar trends, namely, PL quenching (by up to a factor of 0.6) in the case of the thinner shell and PL enhancement (up to a factor of 1.8) for the thicker shell.

There are multiple interaction mechanisms between QDs and metal nanostructures that can influence the PL intensity.[2a,9] One mechanism is due to the modification of the electric field near the metal surface, which changes both the field applied to the QD and the field radiated by it. We account for this effect by introducing factors f_a and f_e defined as $f_a = \sigma^*/\sigma$ and $f_e = \Gamma_r^*/\Gamma_r$, where σ and

10.1021/ja0660296 CCC: $33.50

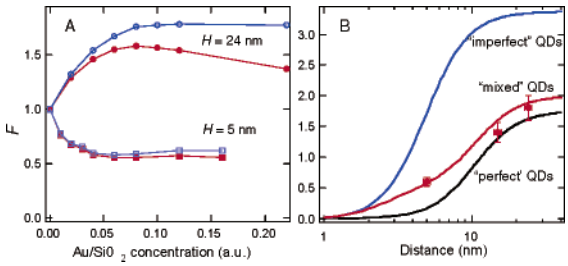

Figure 2. (A) PL quenching/enhancement factors (F) measured as a function of concentration of Au/SiO_2 nanoparticles [D = 45 nm, H = 5 (squares) and 24 nm (circles)]; red solid symbols are raw data and blue open symbols are data corrected for attenuation of pump light. (B) The dependence of F on d for the flat gold surface calculated for three different QD ensembles (see text for details). Symbols are experimental results.

σ^* (Γ_r and Γ_r^*) are QD absorption cross-sections (radiative decay rates) without and with the proximal metal, respectively. Another effect is damping induced by energy transfer from the emitter to the metal (rate Γ_m), which can be described in terms of Joule heating.[2a]

In our experiments, we monitor the change in the emission intensity induced by adsorption of an increasing number of QDs onto Au/SiO_2 nanoparticles for a constant number of QD emitters in the sample and a fixed excitation level. In this case, the PL quenching/enhancement factor, F, can be presented as $F = f_a Q^*/Q$, where Q and Q^* are QYs of the reference QD sample and the Au/SiO_2/QD composite, respectively. For a QD with the intrinsic nonradiative rate Γ_{nr}, $Q = (1 + \gamma_{nr})^{-1}$and $Q^* = f_e(f_e + \gamma_{nr} + \gamma_m)^{-1}$, where $\gamma_{nr} = \Gamma_{nr}/\Gamma_r$ and $\gamma_m = \Gamma_m/\Gamma_r$. For small QD-to-metal distances ($d \ll D/2$), the parameters f_a, f_e, and γ_m can be calculated assuming that the metal surface is a plane.[2a] This assumption provides an accurate approximation for the thinnest (5 nm) shells studied here and is less accurate for the thickest (24 nm) shells. However, it still allows us to obtain useful insights into the mechanisms for QD−metal interactions.

Within the image-charge theory applied to a flat metal surface,[2a] the field enhancement factors f_a and f_e are distance independent and in the case of Au/SiO_2 interface are ~1.8 (at 400 nm) and ~2 (at 630 nm), respectively (averaged over emitting dipole orientations). Damping induced by the metal is, on the other hand, strongly d-dependent and is described by the proportionality $\gamma_m \propto d^{-3}$. The distance dependence of F is determined by whether or not all QDs in the ensemble could be described by a single nonradiative rate Γ_{nr}. The existence of such a rate would imply that the PL decay of the QD sample is single exponential with a total rate ($\Gamma_{nr} + \Gamma_r$). However, previous studies indicate that colloidal QDs exhibit multiexponential PL relaxation,[10] which suggests distribution of rates Γ_{nr}. A simplified description of this distribution is in terms of two QD subensembles of "perfect" ($Q_1 = 1$, $\gamma_{1nr} = 0$) and "imperfect" ($Q_2 < 1$, $\gamma_{2nr} > 0$) dots with relative dot fractions n_1 and n_2 ($n_1 + n_2 = 1$), where n_2 relates to the overall QY of the QD sample by $n_2 = (1 - Q)(1 + \gamma_{2nr-1})$.

In Figure 2B, we show a distance dependence of F calculated for three different cases: (1) "all-perfect" dots ($n_2 = 0$ and $Q = Q_1 = 1$; black line), (2) "all-imperfect" dots ($n_2 = 1$ and $Q = Q_2 = 0.05$; blue line), and (3) a mixed "perfect-imperfect" ensemble ($n_2 = 0.957$, $Q_2 = 7.6 \times 10^{-3}$, $Q = 0.05$; red line). The comparison of these traces indicates a significant effect of heterogeneity in Γ_{nr} on both the absolute magnitude of F and its distance dependence. In case 1, PL enhancement is only possible through the excitation channel; therefore, the maximum value of F (for large d) approaches f_a. In case 2, enhancement is possible through both the absorption and emission channels, which increases the maximum value of F up to ~f_a f_e. Moreover, the role of energy-transfer damping is decreased compared to case 1 because Γ_m competes with a much greater intrinsic relaxation rate determined primarily by Γ_{nr} (if $Q \ll 1$, $\Gamma_{nr} \gg \Gamma_r$); therefore, in case 2 metal-induced damping becomes important at much shorter distances than in case 1.

The computed values of F in case 2 are significantly different from those measured experimentally (symbols in Figure 2B) despite the matching value of Q. This discrepancy clearly indicates the importance of taking into account nonuniformity of nonradiative rates existing in real QD samples. Using a two subensemble model (red line in Figure 2B), we can closely reproduce the experimental results for both thin and thick shells by assuming that $n_2 = 0.957$ and $\gamma_{2nr} = 130$, which correspond to the initial QY of 5%. Since in this model the overall QY of the sample at large d is determined primarily by "perfect" dots, the predicted maximum value of F is close to that in case 1. This consideration implies that in our samples the PL enhancement occurs primarily via the excitation channel (factor f_a).

In conclusion, we have developed a multistep synthesis of hybrid superstructures that comprise gold cores and dense layers of CdSe QDs separated by a silica shell. This architecture allows for versatile control of QD−metal interactions through control of the metal-core size (and potentially core shape and composition) and the thickness of the dielectric spacer. We use these hybrid structures to perform a quantitative analysis of the effect of the metal on QD PL. One important result of this analysis is that nonuniformity of nonradiative rates across the QD ensemble has a significant effect on both the magnitude and the shell-thickness dependence of the PL intensity.

Acknowledgment. This work was supported by the Office of Basic Energy Sciences, U.S. Department of Energy, Center for Integrated Nanotechnologies, and Los Alamos LDRD funds.

Supporting Information Available: Details of synthetic procedures and theoretical modeling of semiconductor−metal interactions in hybrid Au/SiO_2/QD nanostructures. This material is available free of charge via the Internet at http://pubs.acs.org.

References

(1) Raether, H. *Surface Plasmons*; Springer-Verlag: Berlin, 1988; Vol. 111.
(2) (a) Gersten, J.; Nitzan, A. *J. Chem. Phys.* **1981**, *75*, 1139−1152. (b) Nikoobakht, B.; Burda, C.; Braun, M.; Hun, M.; El-Sayed, M. A. *Photochem. Photobiol.* **2002**, *75*, 591−597. (c) Dulkeith, E.; Ringler, M.; Klar, T. A.; Feldmann, J.; Javier, A. M.; Parak, W. J. *Nano Lett.* **2005**, *5*, 585−589. (d) Schneider, G.; Decher, G.; Nerambourg, N.; Praho, R.; Werts, M. H. V.; Blanchard-Desce, M. *Nano Lett.* **2006**, *6*, 530−536. (e) Lee, J.; Govorov, A. O.; Dulka, J.; Kotov, N. A. *Nano Lett.* **2004**, *4*, 2323−2330. (f) Tovmachenko, O. G.; Graf, C.; van den Heuvel, D. J.; van Blaaderen, A.; Gerritsen, H. C. *Adv. Mater.* **2006**, *18*, 91−95.
(3) West, J. L.; Halas, N. J. *Annu. Rev. Biomed. Eng.* **2003**, *5*, 285−297.
(4) Song, J. H.; Atay, T.; Shi, S.; Urabe, H.; Nurmikko, A. V. *Nano Lett.* **2005**, *5*, 1557−1561.
(5) Bergman, D. J.; Stockman, M. I. *Phys. Rev. Lett.* **2003**, *90*, 027402−027404.
(6) Enustun, B. V.; Turkevich, J. *J. Am. Chem. Soc.* **1963**, *85*, 3317−3328.
(7) Liz-Marzan, L. M.; Giersig, M.; Mulvaney, P. *Langmuir* **1996**, *12*, 4329−4335.
(8) Murray, C. B.; Norris, D. J.; Bawendi, M. G. *J. Am. Chem. Soc.* **1993**, *115*, 8706−8715.
(9) Chance, R. R.; Prock, A.; Silbey, R. *Adv. Chem. Phys.* **1978**, *37*, 1−65.
(10) Crooker, S. A.; Barrick, T.; Hollingsworth, J. A.; Klimov, V. I. *Appl. Phys. Lett.* **2003**, *82*, 2793−2795.

JA0660296